



Exploring the probing capacities of MSA capped CdTe semiconductor quantum dots as optical chemsensors via analytical and isotherms modeling for selective Hg²⁺ detection

Mohamed Ajroud¹ · Faiza I. A. Abdella² · Tahani Y. A. Alanazi² · Meryem Helaoui¹ · Sarra Boudriga³

Received: 4 September 2023 / Accepted: 7 December 2023 / Published online: 9 January 2024
© The Author(s) 2024

Abstract

Heavy metal ions bioaccumulation can cause severe damage to environment and human health. Hence, the development of an effective detection assay of trace amounts of these ions is of great importance. Here, CdTe quantum dots (QDs) capped with mercaptosuccinic acid (MSA) ligands have been synthesized in aqueous solution with significant stability and good fluorescence properties. Photophysical characterization was performed using FTIR, XRD, HRTEM and UV–Vis. Absorption, PL and PLRT techniques, seeking their subsequent application as fluorescent probes for metal cations. CdTe-MSA QDs showed selective sensitivity toward Hg²⁺ ions by monitoring quantitative fluorescence quenching with increasing analyte content. Under optimal conditions, the linear range for the detection was 0.2–6 μM with a detection limit of 0.05 μM. According to the Stern–Volmer model, it can be inferred that a static quenching mechanism via Hg²⁺ selective binding to MSA carboxylate groups is operating with electron transfer process. Excess of mercuric ions further decreased and red shifted the fluorescence possibly due to competitive cation exchanges. To further explain the corresponding ligation mechanisms, adsorption behavior study was conducted via several isotherms as well as statistical physics models. The pseudo-first-order model can describe the adsorption kinetics of Hg²⁺ on CdTe-MSA QDs more accurately and the experimental data fitted well the Langmuir isotherm model of monolayer adsorption on homogeneous surface. Furthermore, this spontaneous process conforms to the Hill model as a physisorption with an adsorption energy of 32 kJ.mol⁻¹ associated with the electrostatic interactions and hydrogen bonding. The developed system was assayed in the Hg²⁺ trace amount detection in real tap water and showed satisfactory accuracy performance meeting analytical requirements. The relevant results demonstrated that CdTe-MSA QDs could be deployed as promising Hg²⁺ fluorescent chemosensing system with high sensitivity and selectivity over wide linear detection range that have great potential for real water samples analysis.

Keywords CdTe QDs · Fluorescence quenching · Hg²⁺ Selective detection · Adsorption isotherms, Optical chemsensors

✉ Mohamed Ajroud
mohamed.ajroud50@gmail.com

✉ Sarra Boudriga
sarra_boudriga@yahoo.fr

Faiza I. A. Abdella
fai.ahmed@uoh.edu.sa

Tahani Y. A. Alanazi
ty.alanazi@uoh.edu.sa

¹ Laboratory of Interfaces and Advanced Materials (LR11ES55), Faculty of Science of Monastir, University of Monastir, 5019 Monastir, Tunisia

² Department of Chemistry, College of Science, University of Hail, 81451 Ha'il, Saudi Arabia

³ Laboratory of Heterocyclic Chemistry Natural Product and Reactivity (LR11ES39), Faculty of Science of Monastir, University of Monastir, 5019 Monastir, Tunisia

Introduction

The requirement for developing fluorescent sensors for specific chemical and biological ionic species is continuously increasing since the pollution is becoming a serious global issue for both ecosystems and human health. Various pollutants, derived from human activities, have drawn great concern due to their harmful damage to environment and human beings (Amari et al. 2021; Leitzke et al. 2022). Heavy metal ions, especially mercury ions, have great toxicity because of their highly reactive nature through bioaccumulation even at minor concentrations. This could cause many diseases (kidney failure, nervous system damage, etc.) together with water and soil contamination (Järup 2003; Vinoth Kumar et al. 2018). Therefore, as a response to health concerns and

legal restrictions, development of novel highly efficient and sensitive probes is of particular importance for detecting trace Hg^{2+} amounts in the environment and in biological samples.

Various sensing techniques, such as X-ray fluorescence spectrometry (Sitko et al. 2015), electrochemical voltammetry and potentiometry (Ding et al. 2021), and photoelectrochemical methods (Xu et al. 2022; Shu and Tang 2020), have been deployed and met the requirements of accuracy and sensitivity. However, high cost equipment, large volume and highly precise sample preparation are often intended by most of them. Even so, responding to the growing demand for efficient sensor materials with low cost, high sensitivity, good stability and ease of operation is still a big challenge.

Over the last decades, semiconductor colloidal quantum dots (QDs) have gained considerable interest as fluorescent probes owing to their unique photophysical properties like size-tunable narrow emission bands, across the visible and NIR spectrum, with high photoluminescence efficiency, wide continuous absorption spectra, large Stokes shift, long luminescence lifetime, excellent photostability and ease of functionalization (Wu et al. 2014a, b; Ben Brahim et al. 2017; Du et al. 2017; García De Arquer et al. 2021). Hence, they have been favorably adopted in the fluorescence sensing systems compared to organic dyes which are generally suffering of some drawbacks such as photobleaching and lower response signal. (Xia and Zhu 2007).

Aqueous route synthesized QDs are readily water soluble, biologically compatible and photostable. Notably, their surface modification with appropriate capping ligands not only imparts higher photoluminescence quantum yield (QY) but also would make them available for ionic interactions. This causes analyte induced fluorescence changes taken as sensing response in analysis systems for various applications such as bio-labelling, fluoroimmunoassay and ions sensing (Delehanty et al. 2011; Alibolandi et al. 2014; Chandan et al. 2018; Das and Dutta 2021; Chen and Wu 2014; Ke et al. 2014). Among II–VI QDs, functionalized CdTe generated a widespread interest as probes for multiple targeted species (Wei et al. 2015; Hao et al. 2019; Singh et al. 2020; Ensafi et al. 2016). To enhance affinity and specificity to the analyte, surface modification is inspected with stabilizing capping agent of thiol-based ligands (MPA, GSH, MSA, etc.) (Ribeiro et al. 2019; Cai et al. 2014). They have twofold role: governing the growth of QDs by adequate solubility in the dispersion solution and providing chemical accessibility through functional groups (amine, carboxylate, etc.). The mercaptosuccinic acid (MSA) is recognized as a stabilizer of choice that can provide QDs with high stability and good luminescence performance as well as having two effective $-\text{COOH}$ functional groups giving strong affinity to multiple species (Sousa et al. 2018; Dutta et al. 2015; Hoang et al. 2022). Thus, the MSA molecule functions as

an excellent reagent and stabilizer which predicts prominent sensing characteristics of MSA functionalized CdTe QDs for metal ions probing in aqueous medium. However, their quantitative determination needs further understanding of the photophysical mechanisms governing the sensitive and selective cation detection. In this context and with the aim of obtaining an effective and low-cost nanosensors that can be used at industrial scale, the present work reports the synthesis of MSA capped CdTe QDs and their optical and morphological characterization by UV–Vis. Absorption and photoluminescence spectroscopies as well as FTIR, transmission electron microscopy (TEM) and XRD diffraction techniques. Furthermore, they were evaluated for effectively measuring mercury ion content in water based on the luminescence quenching effect. To a certain extent in the micromolar range, a linear sensitivity toward Hg^{2+} cations with good selectivity is appraised. To the best of our knowledge, few researchers have considered the adsorption characteristics in the sensing process. In a prominent approach, we have applied kinetics studies and equilibrium adsorption isotherms to evaluate the experimental data and to investigate the adsorption characteristics and the detection mechanisms taking into account the influencing parameters such as pH values, metal ion amount and surrounding medium influence.

The proposed probing system was successfully applied to Hg^{2+} ions detection in tap water samples with satisfactory recovery that met the practical requirements. The determined analytical sensing performances favor convenient application of the CdTe-MSA QDs in environmental fields as fluorescence probe for $\text{Hg}(\text{II})$ cations.

Experimental

Reagents

All chemicals, Cd acetate dehydrate $\text{Cd}(\text{CH}_3\text{COO})_2 \cdot 2\text{H}_2\text{O}$, Mercaptosuccinic Acid (MSA) $\text{HOOCCH}(\text{SH})\text{CH}_2\text{COOH}$, tellurium dioxide (TeO_2), NaOH and Sodium tetrahydroborate (NaBH_4), purchased from Sigma–Aldrich (USA), were of analytical grade, no purification process was needed.

Synthesis of aqueous CdTe-MSA quantum dots

CdTe-MSA QDs were synthesized through a colloidal hydrothermal route. In a first step, 6 mmol of Cd acetate dehydrate and 12 mmol of MSA were dissolved in 120 mL of deionized (DI) water. Then, the pH of this mixture was adjusted to 11 using NaOH solution (1M) and the solution was submitted to N_2 bubbling deaeration for 30 min. In the second step, another aqueous solution of TeO_3^{2-} was prepared (1 mmol of TeO_2 in 80 mL of DI water with excess

of NaOH) and added drop wisely to the initial one, with the reducing agent NaBH_4 in excess, with vigorous stirring at 25 °C. The precursors conversion to CdTe QDs is accomplished by refluxing the mixture for 1.5 h under N_2 . Finally, the solution was cooled to the room temperature to stop the QDs growth, then concentrated down to 25 mL using an evaporator.

The mixture was stirred for 1 h at 25 °C, followed by the addition of 20 mL of methanol to precipitate the CdTe QDs nanoparticles which were collected by filtration and dried in a desiccator under vacuum. The used precursors concentrations give a stoichiometric ratio $\text{Cd/MSA/Te} = 6/12/1$, allowing good saturation coverage of the dangling bonds at the QDs surface.

Preparation of metallic ion solutions

The solutions of the metallic ions were prepared by dissolving the corresponding metal salts in DI water. All the inorganic salts, namely LiCl , NaNO_3 , $\text{Ba}(\text{NO}_3)_2$, $\text{Ni}(\text{NO}_3)_2 \cdot 6\text{H}_2\text{O}$, $\text{CoCl}_2 \cdot 6\text{H}_2\text{O}$, $\text{Zn}(\text{NO}_3)_2 \cdot 6\text{H}_2\text{O}$, $\text{Cu}(\text{NO}_3)_2 \cdot 3\text{H}_2\text{O}$, $\text{Fe}(\text{SO}_4)_3 \cdot 7\text{H}_2\text{O}$, $\text{Mn}(\text{SO}_4) \cdot 0.2\text{H}_2\text{O}$, $\text{Cr}(\text{NO}_3)_3$, $\text{Hg}(\text{NO}_3)_2$, KNO_3 and $\text{Mg}(\text{NO}_3)_2$, were purchased from Fluka or Sigma-Aldrich.

We dissolved one millimole of each salt in 10 mL of DI water to obtain 10^{-1} M stock solutions. They were diluted, with adjusted pH, to the desired concentrations as needed.

QDs characterization instruments

The Fourier transform infrared (FTIR) spectra were obtained with a Perkin Elmer FTIR spectrophotometer (version 5.3), at 25 °C, within the $400\text{--}4000\text{ cm}^{-1}$ wavenumber range and using KBr pellets. The x-ray diffraction (XRD) analysis of the synthesized QDs was determined by using a Philips X'Pert PRO.MPD diffractometer using the Cu K_α line ($\lambda = 1,542\text{ \AA}$). High-resolution transmission electron microscopy (HRTEM) characterization was carried out by a Philips CM200 instrument operating at 200 kV accelerating voltage. Samples were analyzed after dropping 10 μL of the nanoparticles solution onto a carbon film left on copper grids and the solvent excess was evaporated. UV-visible absorption study was performed using a SPECORD 210.Plus spectrophotometer at 25 °C, with quartz cuvettes, in the range of $200\text{--}0.800\text{ nm}$. Photoluminescence (PL) measurements were done at 25 °C, using a helium-cadmium laser ($\lambda_{\text{exc}} = 325\text{ nm}$) within a conventional PL setup. Time-resolved photoluminescence (TRPL) measurements were performed by a spectrometer Horiba Fluorolog, having NanoLED (Horiba) as excitation source at 372 nm.

Kinetics and isotherms of Hg^{2+} adsorption experiments

To assess the adsorption properties of Hg^{2+} cations on CdTe QDs, the effect of adsorption time (5–90 min) and initial concentration of $\text{Hg}(\text{II})$ ions ($0.2\text{--}10\text{ }\mu\text{M}$) were investigated. Adsorption and kinetic experiments were carried out at room temperature (298 K) where 1mg of CdTe QDs powder was added to 50 mL of Hg^{2+} aqueous solution with various initial concentrations. The solution pH was adjusted to 7.2 by adding NaOH. After passing the saturation time, the amount of residual mercuric ions in the solution supernatant fraction is measured by a UV-vis spectrophotometer. The equilibrium adsorption capacity Q_e (mg.g^{-1}) is given by the following equation: $Q_e = \frac{(C_0 - C_e)}{m} V$ assuming C_0 (mg.L^{-1}) and C_e (mg.L^{-1}) are the cation initial and residual concentrations, respectively, m (g) is the mass of the CdTe-MSA QDs and V (L) is the solution volume.

To minimize random errors, experiments were repeated three times to yield mean values.

Results and discussion

Structural and chemical characterization of CdTe-MSA QDs

The crystal structure, size distribution and surface functional groups of the prepared CdTe-MSA QDs were investigated using HRTEM, XRD and FTIR techniques. As displayed in HRTEM image (Fig. 1a), the QDs had good monodisperse nature and quasi-spherical shape, having an average diameter of 3.4 nm, deduced from QDs size distribution analysis (Fig. 1b). No reflections attributed to impurities were detected in the pattern proving the high purity of the material.

The existence of well resolved lattice planes, continuous all over the material, clearly reveals the crystal nature of the QDs. The interlayer distance 0.33 nm is close to the standard interplanar distance of the (111) planes in the cubic ZB crystal structure of CdTe (0.37 nm) as given in JCPDS Card No. 75-2086 (Shenouda and El Sayed 2015).

The crystal structure and the QDs mean size could be also determined from the XRD pattern (Fig. 2). The intense and broadened diffraction bands indicate the formation of particles at the nanoscale range.

The major diffraction peaks centered at 2θ equal to 25.3° , 40.6° and 48.9° could be attributed dominantly to, respectively, the (111), (220) and (311) crystallographic planes of the Zinc-blende ZB cubic structure of CdTe, as indexed in literature (Shenouda and El Sayed 2015; Smith et al. 2009). Nevertheless, we cannot neglect the existence of a

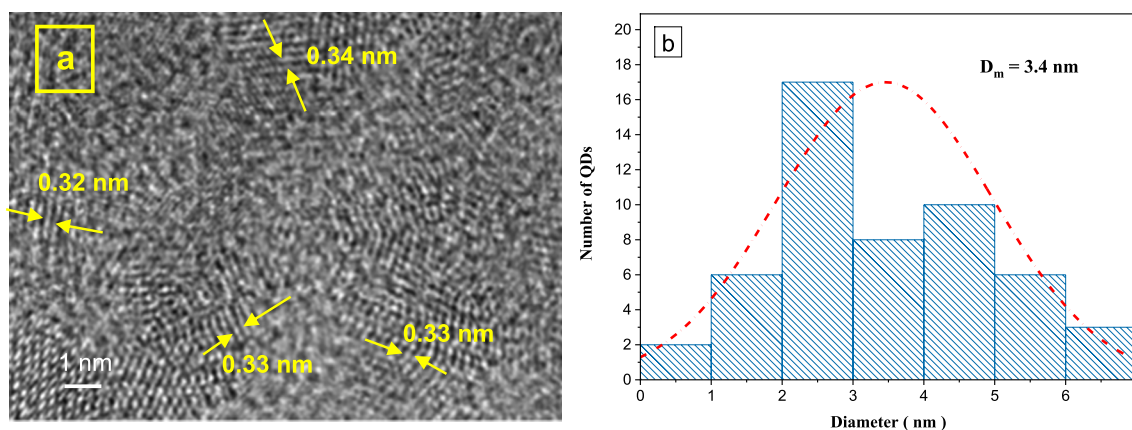


Fig. 1 **a** HRTEM image of CdTe-MSA QDs showing the crystal planes; **b** Size distribution Histogram

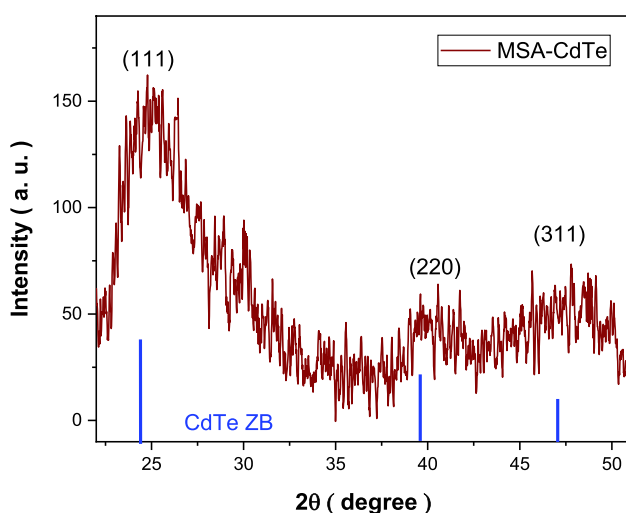


Fig. 2 XRD pattern of CdTe-MSA QDs with the ZB cubic structure peak assignments

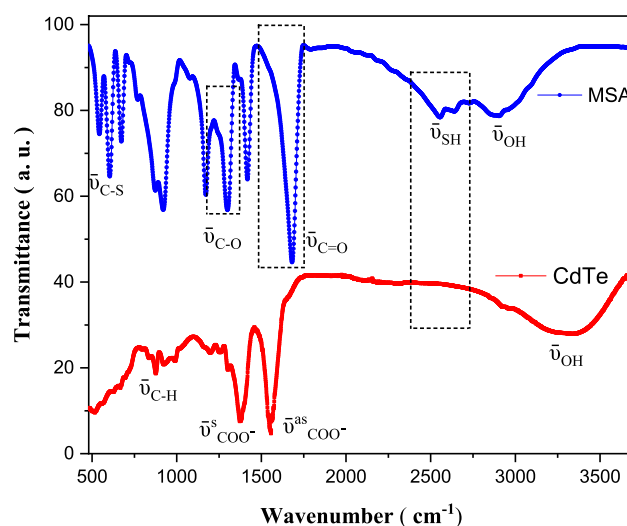


Fig. 3 FTIR spectra of pure MSA and MSA capped CdTe QDs with assignment of major bands

small contribution from the hexagonal phase reflecting the polymorphism nature of these materials. We thought that this polytypism is manifesting in stacking faults of the ZB cubic phase (111) direction due to the tiny energy difference between the two structures (10 meV per atom). Also, the large band centered at nearly 49° is originating from the overlap of (311) ZB planes peak with those of the (103) and (200) planes of the hexagonal system (Smith et al. 2009).

The mean quantum dot diameter D can be estimated by Scherrer's formula (Bel Haj Mohamed et al. 2014) expressed by Eq. (1):

$$D = \frac{K\lambda}{\beta \cos\theta} \quad (1)$$

where $\lambda = 1.54 \text{ \AA}$ is the wavelength of X Rays, $k = 0.9$ is the empirical Scherrer constant, θ is the angular position of the diffraction band (in radians) and β is its full width at half maximum (FWHM).

Relatively to the maximum peak at $2\theta = 25.3^\circ$, assigned to the (111) plane, the average crystal size of CdTe-MSA QDs was estimated to be 3.1 nm. The particle size determined from TEM is rather larger than that given by XRD technique. Since the latter experiences systematic errors, the TEM is held to give more accurate measure (El Nahass et al. 2014).

FTIR measurements shed light on the bindings of the thiol capping ligands to the QDs surface. The resultant spectra of the pure MSA and CdTe-MSA QDs in the 500–4000 cm^{-1} range are shown in Fig. 3.

For the pure MSA ligand, the most pronounced absorption bands occur at 3000 cm^{-1} ($\bar{\nu}_{\text{OH}}$), 2550 cm^{-1} ($\bar{\nu}_{\text{SH}}$), 1680 cm^{-1} ($\bar{\nu}_{\text{C=O}}$), 1290 cm^{-1} ($\bar{\nu}_{\text{C-O}}$) and 630 cm^{-1} ($\bar{\nu}_{\text{C-S}}$).

The ligation of capping MSA chain on the CdTe QDs reveals considerable changes in the FTIR spectrum. Notably, the disappearance of the characteristic thiol (S–H) vibration band, generally observed around 2550 cm^{-1} , indicates the cleavage of this S–H bond and the sulfur atom fixation on the surface of nanoparticles. We infer that a new S–Cd covalent bond on the surface is established due to the strong interaction of sulfur atom electron pair with the cadmium atom, forming thus the capping layer that slows the growth of the quantum dots (Bel Haj Mohamed et al. 2014).

Pure MSA ligands with carboxylic acid groups display a broad –OH stretching band around 3000 cm^{-1} and a C=O asymmetric stretching mode at 1700 cm^{-1} . For the CdTe-MSA QDs, two bands centered at 1420 cm^{-1} and 1566 cm^{-1} appeared and are assigned to the –COO–symmetric and asymmetric stretching vibration modes since at $\text{pH} = 12$, the carboxylic acid groups undergo deprotonation in alkaline medium, given $\text{pK}_{a1} = 3.16$ and $\text{pK}_{a2} = 4.67$, and exists as carboxylate ion. This suggests that the MSA groups are bound to QDs surface leaving the hydrophilic –COO–groups directed outward which makes the surface negatively charged. This feature renders the electrostatic repulsion possible leading to capped QDs soluble and well dispersed in solution (Abdelbar et al. 2016). Furthermore, we could assign the broad band appearing around 3300 cm^{-1} in the CdTe-MSA QDs FTIR spectrum to OH stretching mode of water molecules bound to QDs surface. Another band situated at 900 cm^{-1} is attributed to C–H bending (Liu et al. 2008; Kalsad et al. 2010). These results evidently confirmed the attachment of the capping MSA chain on the QDs surface.

Optical characterization of CdTe-MSA QDs

An immediate evidence of the QDs growth comes from the optical spectra. The absorption profile shows a well resolved excitonic absorption band edge, indicating a relatively narrow QDs size distribution, which is assigned to the characteristic $1S_{3/2} - 1S_e$ electronic transition for the first excitonic state of size quantized CdTe-MSA QDs (Fig. 4a).

The optical band gap energy E_g of QDs depends on the size. The absorption data allows to estimate E_g of the CdTe-MSA QDs according to the Tauc equation given by Eq. (2):

$$\alpha h\nu = A(h\nu - E_g)^n \tag{2}$$

Here, $h\nu$ is the photon energy, α is the absorption coefficient, A is a constant and $n = \frac{1}{2}$ for semiconductors with direct band gap (Tauc and Menth 1972).

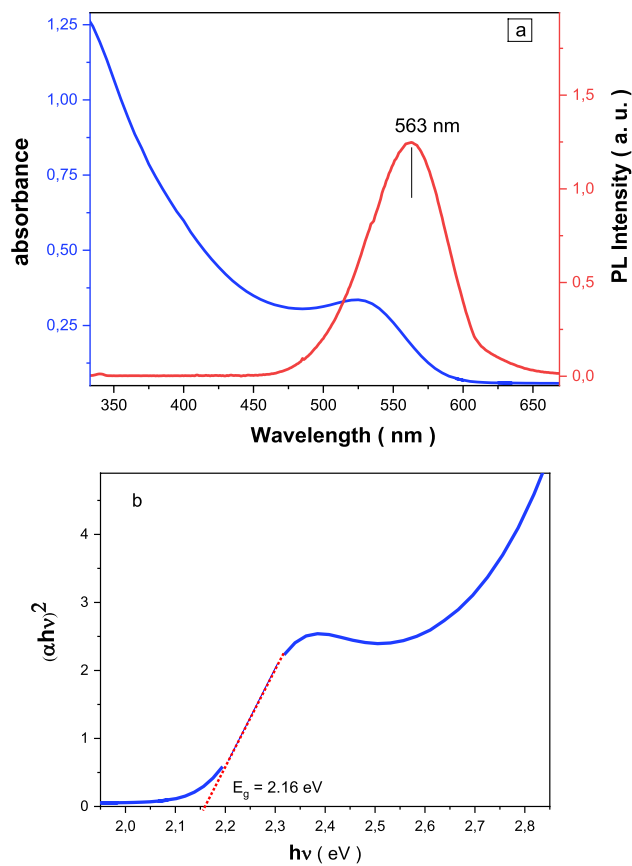


Fig. 4 a UV–vis absorption spectrum (blue line) and emission spectrum (red line, $\lambda_{\text{exc}} = 325\text{ nm}$) of the CdTe-MSA QDs, at $T = 25\text{ }^\circ\text{C}$; **b** Determination of the QDs band gap by Tauc method

Quantitatively, in the plot of the function $(\alpha h\nu)^2$ versus $h\nu$, E_g is determined by the extrapolation of the near edge band tangent to $\alpha = 0$. The intersection with the x -axis yielded the E_g value as $E_g = 2.16\text{ eV}$ which is distinctly blue shifted relative to that of the CdTe bulk (1.5 eV) (Fig. 4b).

This increase in the band gap is attributed to the quantum confinement effect. This behavior becomes more pronounced with decreasing particle size in comparison with the bulk material Bohr exciton radius, resulting in changes in kinetic energy and an increase in the gap energy between allowed states near the absorption edge (Kapitonov et al. 1999; Gogoi et al. 2012).

To correlate nanoparticles band gap energy with their size at the aim of explaining the origin of the blue shift for the quantum confinement regime, Brus proposed the following equation within the effective mass approximation (EMA) (Brus 1986):

$$E_g = E_g^{\text{bulk}} + \frac{h^2}{8r^2} \left(\frac{1}{m_e^*} + \frac{1}{m_h^*} \right) - \frac{1.786}{4\pi\epsilon_0\epsilon_r r} - 0.248E_{Ry}^* \tag{3}$$

Here, E_g is the QDs gap energy, E_g^{bulk} is that of the bulk material and r is the QDs radius. The second term accounts for the kinetic energy term in function of the electron and the hole effective masses, m_e^* and m_h^* , respectively. The third term depicts the electron-hole Coulomb interaction whereas the fourth term, E_{Ry}^* , arises from the electron-hole spatial correlation, which is generally small compared to the last two terms.

To estimate the CdTe-MSA QDs size, a simplified equation was used neglecting the Rydberg term, where the QDs radius was calculated to be $r = 1.9$ nm.

It is obvious that the CdTe QDs are considered in the strong confinement regime since their size is much less than the Bohr exciton radius in the bulk material, $a_B = 7.3$ nm.

We can notice that the sizes deduced from XRD and absorption spectra are slightly different which could be attributed to experimental considerations. In fact, XRD diffractograms were performed with powdered material whereas absorption data were collected for dispersed QDs in aqueous media and processed based on the EMA approximation assuming a spherical geometry (Pejjai et al. 2017).

The PL spectrum of the CdTe-MSA QDs solution under 325 nm excitation at 25 °C reveals an intense band edge emission centered at 563 nm (Fig. 4a), with a FWHM of 67 nm.

Interestingly, it shows a nearly symmetrical profile with very little emission tail in longer wavelength region (around 620 nm) usually assigned to the charge carriers recombination to the surface trap states. This is further confirmed by the rather small Stokes shift, 37 nm, between the absorption maximum and this band which infers that MSA binding reduced surface defects.

The depicted features are essentially assigned to nearly homogeneous QDs of narrow size distribution with lower density of surface states and internal defects acting as non-radiative trap states. In fact, due to higher surface to volume ratio, surface defects are inherent in nanoparticles, leading to unsaturated dangling bonds and interstitials located at the QDs surface. Therewith, the synthesis method, essentially the used stoichiometric ratio of synthetic precursors, caused the formation of punctual defects (vacancies or interstitial atoms) or extended ones (dislocations, aggregates). Acting as capping ligands, MSA molecules not only efficiently improve the QDs stability and water solubility by formation of a Cd-thiol complex layer on their surface but permit also to passivate the surface trap states yielding higher photoluminescence (Ouni et al. 2022; Saikia et al. 2016; Bel Haj Mohamed et al. 2018).

To further investigate the recombination kinetics in the CdTe QDs by time-resolved photoluminescence spectroscopy, we monitored the PL decay at the 563 nm emission peak.

A biexponential function (Eq. (4)) was the best fit to the decay curve (Fig. 5) with relative amplitudes α_i and time constants τ_i :

$$I(t) = \alpha_1 \exp\left(-\frac{t}{\tau_1}\right) + \alpha_2 \exp\left(-\frac{t}{\tau_2}\right) + \text{cst} \quad (4)$$

The faster fluorescence decay component ($\tau_1 = 24$ ns, $\alpha_1 = 68\%$) is attributed to the intrinsic recombination of core states excitons. The longer lifetime ($\tau_2 = 172$ ns, $\alpha_2 = 32\%$) is associated with surface states recombination (Ben Brahim et al. 2017). The average life time τ_{av} was calculated, using $\tau_{av} = \frac{\sum \alpha_i \tau_i^2}{\sum \alpha_i \tau_i}$, to be 138 ns. This relatively long lifetime is an essential property for potential probes in chemical and biological sensing applications.

Interaction of the CdTe-MSA QDs with metal ions and specificity for Hg^{2+}

The synthesized CdTe-MSA QDs witness many interesting characteristics, high photoluminescence, good photostability, appropriate surface passivation and long lifetime, making them potential candidates for sensing experiments using fluorescence measurements. Thus, we attempted to evaluate the analytical potential of our material as metal ions probes in water. In fact, the carboxylate groups in thiols have high affinity to these targets so that QDs can coordinate efficiently. With various metal ions, such as Cu^{2+} , Hg^{2+} , Ag^+ and Co^{2+} , it induces fluorescence modulation, quenching or enhancement, upon ion binding with surface ligands accompanied by energy transfer, electron transfer and competitive cation exchange (Ribeiro et al. 2019; Labej et al. 2018; Peng et al. 2018; Wang et al. 2016a, b; Lou et al. 2014).

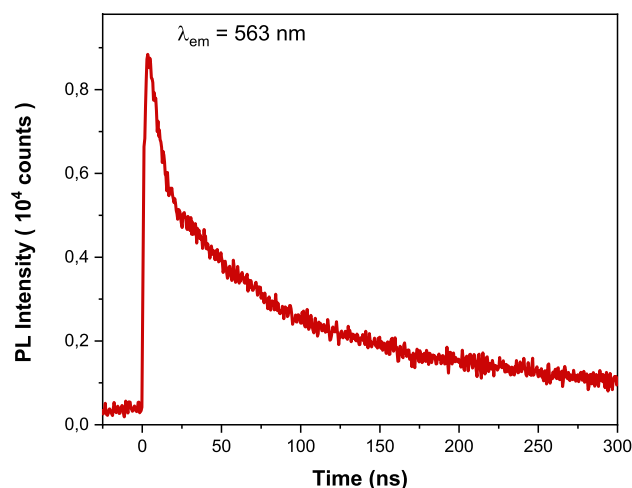


Fig. 5 PL decay curve of CdTe-MSA QDs measured at $\lambda_{\text{max}} = 563$ nm

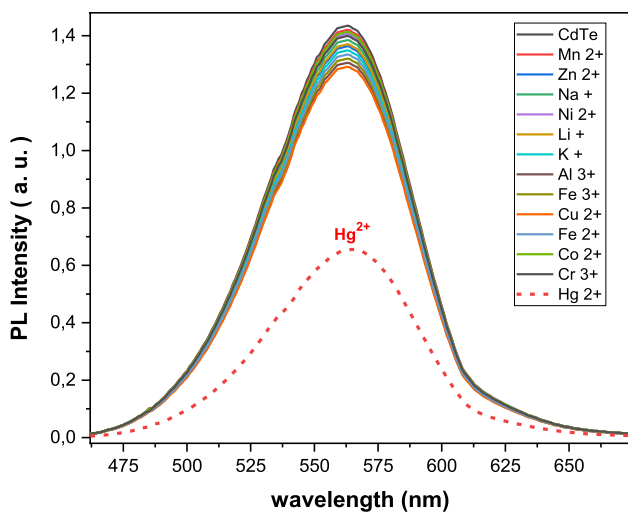


Fig. 6 PL spectra of the CdTe-MSA QDs solution ($0.02 \text{ g}\cdot\text{L}^{-1}$) before and after adding various metal cations ($2 \mu\text{M}$)

In our work, we investigated the response of CdTe-MSA QDs toward various metallic ions by monitoring their fluorescence intensity. Among various metal cations tested at $2 \mu\text{M}$ concentration (Mn^{2+} , Hg^{2+} , Zn^{2+} , Na^+ , Li^+ , Ni^{2+} , K^+ , Al^{3+} , Fe^{3+} , Cu^{2+} , Co^{2+} , Cr^{3+} , Fe^{2+}), only Hg^{2+} ions addition induced a drastic fluorescence quenching of the QDs aqueous solution ($0.02 \text{ g}\cdot\text{L}^{-1}$) (Fig. 6). A very small fluorescence decrease is observed upon adding other metal cations. It was concluded that only Hg^{2+} ions could significantly complex with the CdTe-MSA QDs changing thus the surface chemical properties. Hence, the PL intensity can be monitored as the sensor signal to detect specifically this ion in water.

Fluorescence measurements of CdTe-MSA QDs for detection of Hg^{2+}

With the aim to reach the highest sensitivity permitting the analysis of samples with low concentrations, we have studied the pH effect on the fluorescence in the experimental sensing of CdTe QDs toward Hg(II) ions. In fact, with a special structure, having two carboxylate groups, MSA ligands need further attention not to weaken their passivating abilities for higher PL efficiency when maximizing their binding potential.

The pH effect on the PL intensity of CdTe-MSA QDs was investigated by measuring the relative fluorescence intensity $\frac{F_0}{F}$ vs the varying pH from 2 to 12, where F and F_0 are the analytical fluorescence signal obtained in the presence and absence of Hg^{2+} ions, respectively.

The obtained results, depicted in Fig. 7, showed a PL quenching effect due to Hg^{2+} ions that evolved with the

increase in pH from 4 to 7 then decreased with superior pH values.

When the pH is low in acidic medium, the surface-binding thiolate groups get protonated with increasing H^+ which results in a decomposition of the MSA- Cd^{2+} complex annulus and the loss of coordination to QDs surface. That lower capping induces QDs aggregation and a higher density of nonradiative trap states that causes a small PL response.

At neutral pH, the carboxylic acid groups of MSA with $\text{pK}_{a1} = 3.16$ and $\text{pK}_{a2} = 4.67$ undergo deprotonation which likely strengthens the covalent binding between the thiols and Cd^{2+} at the QDs surface, increasing thus the luminescence.

In alkaline medium $\text{pH} > 7$, as further deprotonation occurs, that leads to more carboxylate ions COO^- with greater charge on the surface of QDs augmenting hence their dispersion in aqueous solution. The diminishing of the fluorescence quenching may be attributed to the formation of a coating hydrated product, $\text{Cd}(\text{OH})_2$ after interaction of OH^- in the solution with Cd^{2+} ions on the CdTe QDs surface (Algar and Krull 2007; Wang et al. 2008; Gan et al. 2012).

As a result, we have performed all sensing experiments in standard conditions at $\text{pH} = 7.2$ with Tris-HCl buffer. The solutions were added in the order: CdTe QDs succeeded by Tris-HCl buffer and then mercury ions, with uniformly mixing for 5 min.

The PL properties of the synthesized CdTe-MSA QDs were studied upon the interaction with different Hg^{2+} ion solutions at increasing concentrations. The pure CdTe QDs exhibited a nearly symmetric peak at 563 nm that was monitored with gradual ions introduction under optimum conditions. The results depicted in Fig. 8a revealed that the emission intensity have gradually declined with the increasing

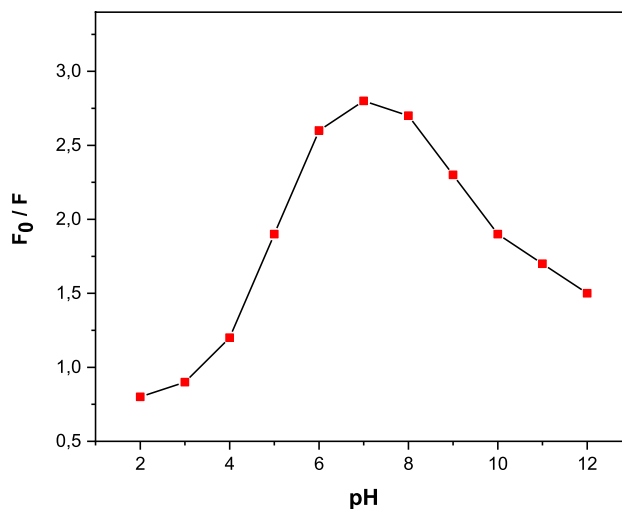


Fig. 7 pH effect on the PL quenching of CdTe-MSA QDs ($0.02 \text{ g}\cdot\text{L}^{-1}$) upon the interaction with Hg(II) ions ($2 \mu\text{M}$)

Hg^{2+} content (0.2, 0.4, 0.6, 0.8, 1, 2, 3, 4, 5, 6, 8, 9 and 10 μM) and almost completely quenched at 12 μM of Hg^{2+} concentration.

Moreover, a slight red shift of the emission band occurred, up to 8 nm at total quenching, without obvious changes in the spectral widths. This fluorescence feature could be ascribed to the strong interaction between the CdTe-MSA QDs and Hg^{2+} cations that could change the surface chemical properties, resulting in the PL quenching. These results constitute a first approach demonstrating that CdTe-MSA QDs are suitable for an effective detection of Hg^{2+} ions in solution that requires a deeper investigation of its mechanisms.

Fluorescence quenching of QDs by metal ions results from either a dynamic process or a static one but in many

instances both of them occur simultaneously. The main feature in a static quenching mechanism consists of forming a ground state complex: fluorescent probe—quencher ion, which is non-emissive, by binding with surface ligands due to their strong affinity. In dynamic process, collisional encounters fluorophore—metal ion results in electron transfer and energy transfer via excited states leading to nonradiative electron–hole recombination at the surface functional groups and metal ions leading to PL quenching.

To explore the PL quenching mechanism, we have applied the Stern–Volmer model described by the following equation (Labej et al. 2018):

$$\frac{F_0}{F} = 1 + K_{sv}[Q] \quad (5)$$

In this expression, F_0 and F are the PL intensities of the fluorophore in the absence and presence of the quenching Hg^{2+} ions, respectively, K_{sv} is the Stern–Volmer constant and $[Q]$ is the quencher concentration.

For purely static or dynamic process, the dependence of PL intensity ratio $\frac{F_0}{F}$ on quencher ion concentration is linear but in many circumstances, an upward curvature with concavity toward the y axis is observed attesting that both mechanisms occur together with the same quencher.

In our experiment circumstances, the Stern–Volmer plot of $\frac{F_0}{F}$ versus $[\text{Hg}^{2+}]$ (Fig. 8b) revealed good linearity (correlation coefficient $R^2 = 0.9906$) for the Hg (II) ions concentration ranging from 0.2 to 6 μM . This suggests that a single class of receptor sites with uniform energy was equally accessible to all metal ions (Bel Haj Mohamed et al. 2018). The K_{sv} constant, representing the quenching efficiency, was calculated from the linearized equation to be: $K_{sv} = 1.32 \cdot 10^6 \text{ M}^{-1}$.

For concentrations higher than 6 μM , the S–V plot reaches a plateau indicating that binding sites get saturated for quencher ions. A limit of detection (LOD) for Hg^{2+} ions was estimated to be 0.05 μM in the operative conditions. Up to the IUPAC definition as $3\alpha/K$, it is the analyte concentration which produces a response signal equal to 3 times the α blank measurements standard deviation. ($n = 10$) where K is calibration graph slope (Shrivastava and Gupta 2011).

The quenching rate constant defined as $K_q = \frac{K_{sv}}{\tau_{av}}$, where τ_{av} is the average PL decay time without quencher ions (138 ns) was then calculated to be $K_q = 9.6 \cdot 10^{12} \text{ M}^{-1} \cdot \text{s}^{-1}$. This value is higher than the maximum diffusion collision quenching constant reported for a collision mechanism, $2.0 \cdot 10^{10} \text{ M}^{-1} \cdot \text{s}^{-1}$. Hence, it is suggested that the quenching mechanism is static in nature, not dynamic, and is initiated by the formation of a nonfluorescent ground state complex between Hg^{2+} ions and QDs ligands (Bel Haj Mohamed et al. 2018).

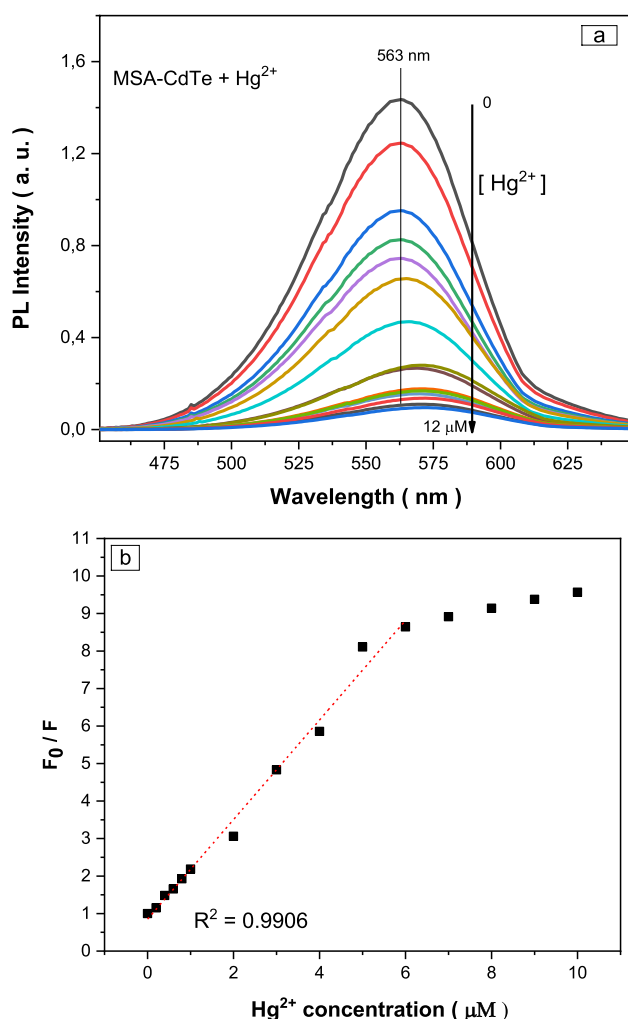


Fig. 8 a Increasing Hg^{2+} concentration effect on the CdTe-MSA QDs PL at 25 °C, in buffer at pH 7.2. Excitation wavelength $\lambda_{ex} = 325 \text{ nm}$; b Stern–Volmer plot of the fluorescence quenching of CdTe-MSA QDs dependence on Hg^{2+} concentration

Interaction mechanisms between Hg^{2+} and CdTe QDs

Changes in the surface chemistry of QDs are closely related to the efficient fluorescence quenching attributed to mechanisms of ion binding followed by electron transfer and competition of ligands.

In this system, electrostatic interaction between quencher ions and the abundant carboxylate groups of the capping MSA ligands on QDs surface lead to the formation of a static complex between Hg^{2+} and CdTe QDs by coordination interaction that quenches the fluorescence.

Most likely, at lower Hg^{2+} concentration, these ions bind onto the surface of QDs through the functional carboxylate groups of MSA, facilitating the electron transfer from conduction band (CB) excited states to $\text{Hg}(\text{II})$ ions. An inhibition of the fluorescence is then observed due to the annihilation of the proper electron–hole recombination of QDs (Fig. 9).

When Hg^{2+} concentration further increases, not only the fluorescence decrease continued but the maximum emission wavelength is red shifted too, which denotes that the surface chemistry of QDs has been changed. In addition to electron transfer which is always acting, a competition of ligands is put forward. In this mechanism, it is thought that Hg^{2+} destroys partially the QDs–ligand Cd–S bond and enter into competition to coordinate with the sulfur atom of the ligand since the solubility constant of HgS ($K_{sp} = 4 \cdot 10^{-53}$) is much lower than that of CdS ($K_{sp} = 8 \cdot 10^{-27}$) indicating that $\text{Hg}(\text{II})$ ions have higher affinity toward -S- group (Label

et al. 2018; Wu et al. 2014a, b). They could form more stable HgS sulfide by replacing Cd^{2+} and some MSA ligands could detach from the surface leading to the charge transfer cut off through Cd–S bond and hence QDs fluorescence quenching (Fig. 9).

Moreover, a small proportion of QDs could merge after addition of Hg^{2+} ions which increases the size slightly and causes fluorescence red shift. Nevertheless, the extent of the red shift (8 nm) and the unchanging HRET spectra suggest that it was not so relevant to generate obvious aggregation (Gong et al. 2016).

The quenching behavior of QDs might also be attributed to alloy layer formation. In fact, due to considerably HgTe low solubility, almost 20 times lower than that of CdTe (Label et al. 2018), superficial substitution of Cd^{2+} by Hg^{2+} ions in QDs results in the formation of an ultra-small $\text{Cd}_x\text{Hg}_{1-x}\text{Te}$ alloyed layer which barely increases the original QDs size. Nevertheless, this new structure imparts red shift and gives rise to more surface defect states leading to the emission quenching by nonradiative recombination pathways (Label et al. 2018; He et al. 2022; Pei et al. 2012; Preeyanka and Sarkar 2021).

Adsorption studies

For further comprehension of the detection mechanism in the fluorescence sensing process, analyzing the adsorption of Hg^{2+} cations on CdTe-MSA receptor sites and determining their rate are vital for the evaluation of the sensor materials performance in practical applications (Deng et al. 2023).

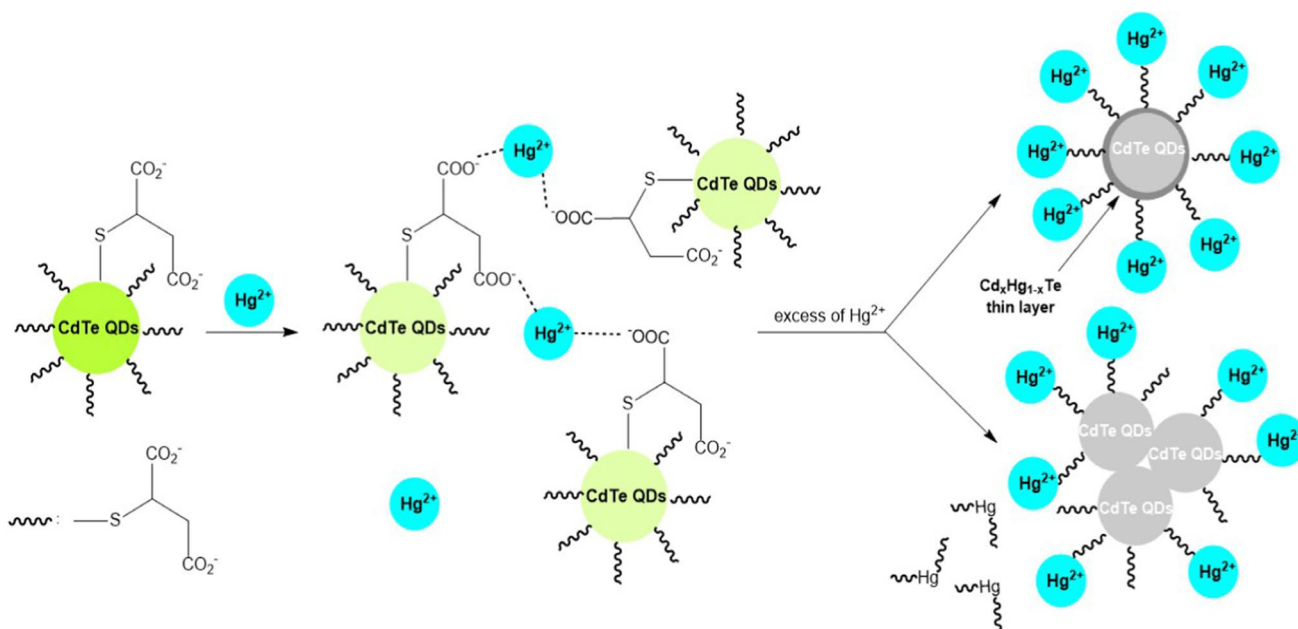


Fig. 9 Proposed mechanisms of coordination interaction between CdTe-MSA QDs and Hg^{2+} ions at low and higher concentrations

Adsorption behavior is analyzed via kinetics study and adsorption isotherms models.

Adsorption kinetics

The influence of the contact time on adsorption capacity is studied with the pseudo-first-order and pseudo-second-order kinetic models which have been widely applied to correlate the experimental adsorption data. They are given by the following equations (Mahmoud et al. 2022; Benjelloun et al. 2021):

The pseudo-first-order kinetic model:

$$Q_1(t) = Q_e [1 - \exp(-K_1 t)] \quad (6)$$

The pseudo-second-order kinetic model:

$$Q_2(t) = \frac{Q_e^2 K_2 t}{1 + Q_e K_2 t} \quad (7)$$

where Q_e ($\text{mg}\cdot\text{g}^{-1}$) is the adsorption capacity at equilibrium and $Q(t)$ ($\text{mg}\cdot\text{g}^{-1}$) that at a certain time t (mn), representing the amount of adsorbed cation. K_1 (min^{-1}) and K_2 ($\text{mg}^{-1}\cdot\text{g}\cdot\text{min}^{-1}$) are the corresponding adsorption rate constants.

Regarding kinetics study for the Hg^{2+} adsorption on CdTe-MSA QDs, conducted at 298 K, data fitting results are presented in Fig. 10.

As seen, two distinct phases governed the adsorption process. First, Hg^{2+} ions were adsorbed rapidly by the CdTe-MSA QDs in the first 20 min, due to the presence of numerous adsorption sites on the nanocrystal surface. Functional carboxylate groups could coordinate mercuric cations via

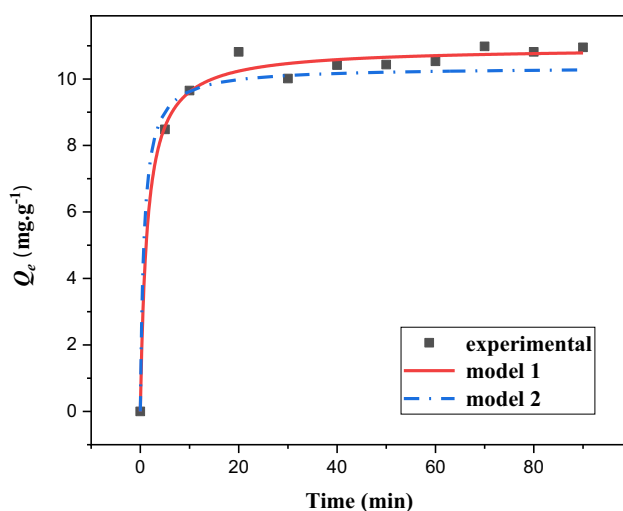


Fig. 10 Kinetics for the Hg^{2+} adsorption on CdTe-MSA QDs and its modeling with the pseudo-first-order equation (model 1) and pseudo-second-order equation (model 2)

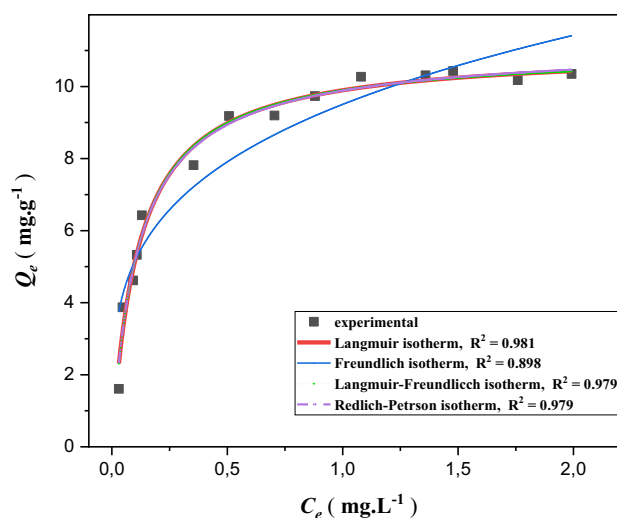


Fig. 11 Adsorption isotherms of Hg^{2+} on CdTe-MSA QDs at pH=7 and 298 K

electrostatic interaction and hydrogen bonding, permitting a rapid and significant diffusion mass transfer gradient of Hg^{2+} on the CdTe-MSA surface.

In a subsequent stage, the adsorption rate slowed down until reaching an equilibrium at about 90 min. In fact, gradually less and less adsorption sites are available on the QDs surface as well as repulsive forces between the adsorbed and free Hg^{2+} ions act simultaneously (Deng et al. 2023).

The application of the pseudo-second-order model gave poor correlation results with predicted Q_e values that did not fit well with the experimental data with low correlation coefficient R^2 value (0.978).

The pseudo-first-order kinetic model was characterized by a higher R^2 value (0.991) and a calculated adsorption capacity ($Q_{1e,cal}$) = 10.71 $\text{mg}\cdot\text{g}^{-1}$, which is close enough to the experimental value ($Q_{e,exp}$) = 10.85 $\text{mg}\cdot\text{g}^{-1}$.

Hence, we can conclude that the Hg^{2+} adsorption kinetics agree reasonably well with a pseudo-first-order model with an adsorption rate constant $K_1 = 0.306 \text{ min}^{-1}$, giving an adsorption relaxation time ($\tau = \frac{1}{K_1}$) of approximately 3.26 min at the temperature $T = 298 \text{ K}$.

Adsorption isotherms

The adsorption behavior was analyzed by four different linear and nonlinear isotherm expressions via Langmuir/Freundlich and Redlich–Peterson models to figure out the interaction mechanisms of Hg^{2+} cations with the surface of CdTe-MSA QDs. In fact, the distribution of these adsorbate species between the solution and the sorbent is determined by the adsorption isotherms. The plots of the experimental data and

their fitting models are depicted in Fig. 11 and the computed parameters are listed in Table 1.

The Langmuir model assumes monolayer adsorption process on homogeneous surface having a definite number of adsorption sites of equivalent energy with no lateral interaction between adsorbate molecules (Langmuir 2018).

This model can be described by the following equation (Foo and Hameed 2010):

$$Q_e = Q_{\max} \frac{K_e C_e}{1 + K_e C_e} \tag{8}$$

At adsorption equilibrium, the Hg^{2+} cation concentration in solution is denoted as C_e ($mg.L^{-1}$), Q_e ($mg.g^{-1}$) is the corresponding adsorption capacity and Q_{\max} ($mg.g^{-1}$) stands for the maximum monolayer adsorption capacity of CdTe-MSA QDs with K_e ($L.mg^{-1}$) as the equilibrium adsorption constant.

As stated in Table 1 and shown in Fig. 11, the Langmuir adsorption isotherm provided a good correlation according to R^2 value of 0.981, where the maximum adsorption capacity determined from this model $Q_{\max} = 10.34 mg.g^{-1}$ is too close to the experimental value of $10.41 mg.g^{-1}$.

The equilibrium adsorption constant value $K_e = 8.78 L.mg^{-1}$ indicates strong adsorbate–adsorbent interaction (Ribeiro et al. 2019).

An important feature often used in the Langmuir model is the dimensionless separation factor R_L whose value permits to anticipate the nature of the adsorption process that could be either favorable adsorption ($0 < R_L < 1$), unfavorable process ($R_L > 1$), linear adsorption ($R_L = 1$) or irreversible process ($R_L = 0$).

The separation factor R_L is expressed by Eq. (9) (Ragadhita et al. 2021):

$$R_L = \frac{1}{1 + K_e C_0} \tag{9}$$

Table 1 Parameters of the isotherm models for Hg^{2+} adsorption on CdTe-MSA QDs

Langmuir isotherm ($R^2=0.981$)	$K_e(L.mg^{-1})$	
$Q_{\max}(mg.g^{-1})$	8.78	
10.34		
Freundlich isotherm ($R^2=0.898$)	$1/n_F$	
$k_f((mg.g^{-1})(mg^{-1}.L)^{\frac{1}{n_F}})$	0.265	
3.80		
Redlich–Peterson isotherm ($R^2=0.979$)	$a_R((mg^{-1}.L)^\beta)$	β
$K_R(L.g^{-1})$	9.844	0.991
39.71		
Langmuir–Freundlich isotherm ($R^2=0.979$)	$K_{LF}(L.mg^{-1})$	n_{LF}
$Q_{\max}(mg.g^{-1})$	8.57	0.996
10.31		

here, C_0 is $Hg(II)$ initial concentration and K_e is Langmuir adsorption constant that yield the value $R_L=0.79$, indicating a favorable normal adsorption process.

The two-parameter Freundlich isotherm model describes the occurrence of a multilayer adsorption on a heterogeneous surface where stronger adsorbate binding sites are occupied first.

It is expressed as follows (Freundlich 1907):

$$Q_e = k_f C_e^{1/n_F} \tag{10}$$

At adsorption equilibrium, C_e ($mg.L^{-1}$) is the Hg^{2+} concentration in solution, Q_e ($mg.g^{-1}$) is the corresponding adsorption capacity, $k_f \left((mg.g^{-1})(mg^{-1}.L)^{\frac{1}{n_F}} \right)$ is the Freundlich adsorption capacity constant and n_F is the Freundlich exponent relative to the intensity of adsorption where $n_F \in [1, 10]$ indicates a favorable adsorption.

Despite the value $\frac{1}{n_F} \sim 0.265$ confirming a favorable Hg^{2+} adsorption by this model, the Freundlich isotherm has poor correlation results since it does not fit well the experimental data and slightly diverges for higher concentrations. Furthermore, its regression coefficient $R^2=0.898$ is smaller than that of Langmuir model.

To additionally describe the adsorption of $Hg(II)$ cations on CdTe QDs, Redlich–Peterson model was used combining elements from both Langmuir and Freundlich models. It represents an adsorption mechanism that does not follow ideal monolayer, over a wide range of concentration of adsorbate and which is applicable in either homogenous or heterogeneous systems. This model is expressed by the following equation (Redlich and Peterson 1959):

$$Q_e = \frac{K_R C_e}{1 + a_R C_e^\beta} \tag{11}$$

In this equation, K_R ($L.g^{-1}$) is Redlich–Peterson constant, a_R ($(mg^{-1}.L)^\beta$) is a constant and β is an exponent whose value is between 0 and 1. When β approaches 1, the adsorption behavior aligns with the Langmuir model, while for β approaching 0, the model reduces to the Freundlich model.

Upon data fitting, the Redlich–Peterson isotherm yielded $R^2=0.979$ and a value of β approximately unity (0.991). These results confirm the model's strong correlation with a Langmuir-type isotherm and further supports the predominance of monolayer formation on a homogeneous adsorbent surface with nearly uniform energies of adsorption.

Lastly, the Langmuir–Freundlich (L–F) isotherm was employed to simulate the adsorption equilibrium data. It is a versatile model that characterizes the distribution of adsorption sites energy onto heterogeneous adsorbent surface. Mathematically, it is expressed as follows (Abu-Alsoud et al. 2020):

$$Q_e = \frac{Q_{\max}(K_{LF}C_e)^{n_{LF}}}{1 + (K_{LF}C_e)^{n_{LF}}} \quad (12)$$

where K_{LF} is the affinity constant for adsorption and n_{LF} is the heterogeneity index that lies between 0 and 1.

At low adsorbate concentration, this model approaches the Freundlich isotherm one, whereas for higher concentration it becomes the Langmuir isotherm.

The calculated L–F parameters were $Q_{\max} = 10.41 \text{ mg.g}^{-1}$ and $K_{LF} = 8.58 \text{ L.mg}^{-1}$ with a regression coefficient $R^2 = 0.979$ which is lower than that of Langmuir isotherm.

As a conclusion, it was found that the isotherm experimental data were best fitted with Langmuir model having the highest $R^2 = 0.981$. Since it is the most suitable in representing the adsorption process, we can suggest that the CdTe-MSA QDs adsorbent surface inculcates monolayer coverage with homogeneous active sites of uniform energy. These receptor sites adsorbate Hg^{2+} cations via weak interaction forces such as electrostatic interaction and hydrogen bonding (Yusuff et al. 2019).

Statistical physics modeling

For deeper analysis of the Hg^{2+} adsorption process by CdTe-MSA QDS, statistical physics isotherms models were applied to determine additionally some physicochemical parameters describing their interaction: the density of adsorption sites (D_s), the corresponding adsorption energies and the number of adsorbed cation per adsorption site (n).

Among them, the Hill adsorption model was applied assuming a monolayer adsorption process of single adsorption energy in which the receptor site can attach one or more than one cation as well as a fraction of a cation (Bouzid et al. 2019). Further explorations lead to other statistical physics models that studied the adsorption of cations involving the formation of two layers, considering one or two different adsorption energies relative to adsorbate–adsorbent interactions and adsorbate–adsorbate interactions, each adsorption site can accept a variable number of cations (Pang et al. 2020).

The evolution of the equilibrium adsorption capacity Q_e , versus the cation concentration C_e within these models are given by the following equations (Pang et al. 2020):

◆ Monolayer process:

$$Q_e = \frac{nD_s}{1 + \left(\frac{C_{1/2}}{C_e}\right)^n} \quad (13)$$

◆ Double layer process with one adsorption energy:

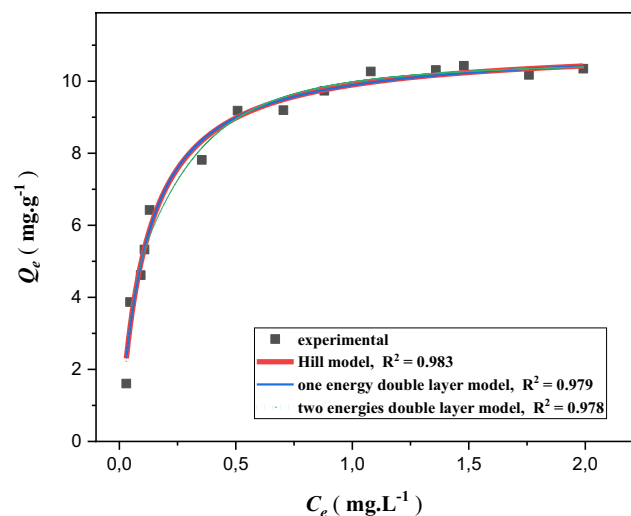


Fig. 12 Statistical physics modeling of adsorption isotherm for Hg^{2+} on CdTe-MSA QDs at 298 K and $\text{pH} = 7$

Table 2 Data correlation results of the statistical physics models applied to the adsorption isotherm of Hg^{2+} on CdTe-MSA QDs at $T = 298 \text{ K}$

Isotherm model	R^2	RMSE
Hill model	0.983	0.0285
Two layers with one energy model	0.979	0.0312
Two layers with two energies model	0.978	0.0312

$$Q_e = nD_s \frac{\left(\frac{C_e}{C_1}\right)^n + 2\left(\frac{C_e}{C_1}\right)^{2n}}{1 + \left(\frac{C_e}{C_1}\right)^n + \left(\frac{C_e}{C_1}\right)^{2n}} \quad (14)$$

◆ Double layer process with two adsorption energies:

$$Q_e = nD_s \frac{\left(\frac{C_e}{C_1}\right)^n + 2\left(\frac{C_e}{C_2}\right)^{2n}}{1 + \left(\frac{C_e}{C_1}\right)^n + \left(\frac{C_e}{C_2}\right)^{2n}} \quad (15)$$

Here, D_s represents the density of receptor sites on the adsorbent surface, n stands for the number of anchored cation per receptor site and $C_{1/2}$, C_1 and C_2 are the cation concentrations at half-saturation for each process, respectively.

The latter three models have been used to fit the experimental adsorption data with the aim of studying the adsorption mechanism of Hg^{2+} cations on the CdTe-MSA QDs. The corresponding plots and fitting parameters are depicted in Fig. 12 and Table 2.

The correlation parameters relative to the monolayer Hill adsorption model ($R^2 = 0.983$ and $\text{RMSE} = 0.0285$) show that the best fit is described by its equation revealing that a

Table 3 Hill model steric and energetic parameters calculated for the Hg²⁺ adsorption on CdTe-MSA QDS at 298 K

<i>n</i>	<i>D_s</i> (mg.g ⁻¹)	<i>Q_s</i> (mg.g ⁻¹)	<i>C_{1/2}</i> (mg.L ⁻¹)	Δ <i>E</i> (kJ.mol ⁻¹)
1.03	4.27	10.40	0.113	32.84

uniform monolayer with the same uptake energy for Hg²⁺ ions is covering the adsorbent surface upon adsorption.

Adsorption energy calculated by the Hill model is related to the half-saturation concentration *C_{1/2}* as expressed by the following nonlinear equation (Bouزيد et al. 2019; Pang et al. 2020):

$$\Delta E = RT \ln \left[\frac{C_s}{C_{1/2}} \right] \tag{16}$$

where *C_s* is the cation precursor molecule solubility (i.e., 65 g.L⁻¹ for HgCl₂), *R* is the universal ideal gas constant (8.314 10⁻³ kJ K⁻¹ mol⁻¹) and *T* is the adsorption temperature (T = 298 K).

Adsorption data fitting parameters upon applying this statistical physics model are given in Table 3.

The obtained results revealed a density of adsorption sites *D_s* equal to 4.27 mg.g⁻¹ and *n* = 1.03, suggesting that one Hg²⁺ cation is linked to one receptor site of CdTe-MSA QDs.

The calculated adsorption energy Δ*E* = 32.84 kJ.mol⁻¹ is lower than 40 kJ/mol, which corresponds to a physical adsorption process.

On the basis of the above results, we can conclude that a parallel adsorption orientation of one cation per receptor site prevailed for the linkage of Hg²⁺ ions on homogenous CdTe-MSA QDs surface with their functional groups as physisorption through hydrogen-bonding and weak electrostatic forces.

Selectivity

Besides sensitivity, selectivity is a crucial parameter for designing an optimal sensor for an analytical procedure. In fact, to be applicable as a probing system for Hg²⁺ ions, CdTe-MSA QDs must function efficiently alike in the presence of other cations.

Under the optimal experimental conditions, the selectivity of the interlinkage probe-analyte was studied by monitoring, at the 563 nm maximum fluorescence wavelength, the CdTe-MSA QDs response toward Hg²⁺ ions both in the absence and the presence of possibly interfering cations (Mn²⁺, Zn²⁺, Na⁺, Ni²⁺, Li⁺, K⁺, Al³⁺, Fe³⁺, Cu²⁺, Fe²⁺, Co²⁺, Cr³⁺). These ions may interfere with Hg²⁺ ions and lead to fluorescence quenching due to possibly formation of insoluble salts or QDs aggregation (Zhou et al. 2022).

For a 3 μM Hg²⁺ solution with the simultaneous presence of various cations at 10 μM concentration, the fluorescence spectra revealed little changes in the intensity compared to that in the absence of competing metallic cations (≤ 5%). As shown with the interference bar diagrams (Fig. 13), the result indicates that the Hg²⁺ ion selective binding is predominant when occurring with coexistence of competing metal ions which have negligible influence.

As a conclusion, the CdTe-MSA QDs probe system shows superior specificity and good selectivity for Hg²⁺ ions within the measurement range, a high-priority feature for sensing experiments in solution that must be very useful in the analysis of complex samples.

Comparative study

The analytical performance of the synthesized CdTe-MSA QDs for mercury ions detection was compared with some previously reported works as summarized in Table 4. It can be inferred that the performance parameters in our study are comparable or even better than some of reported fluorescence probes. Thus, high sensitivity and good selectivity for Hg²⁺ ions together with wide linear detection range and low detection limit make the CdTe-MSA QDs good candidates for use as fluorescence probe to quantitatively and selectively detect Hg²⁺ ions in aqueous media.

Detection of Hg²⁺ in real water samples

To investigate the practical application of our sensor system, real tap water samples were tested by spiking experiments for detection analysis. To this end, three replicate average recovery tests, by monitoring the fluorescence quenching, were performed on these samples spiked with different

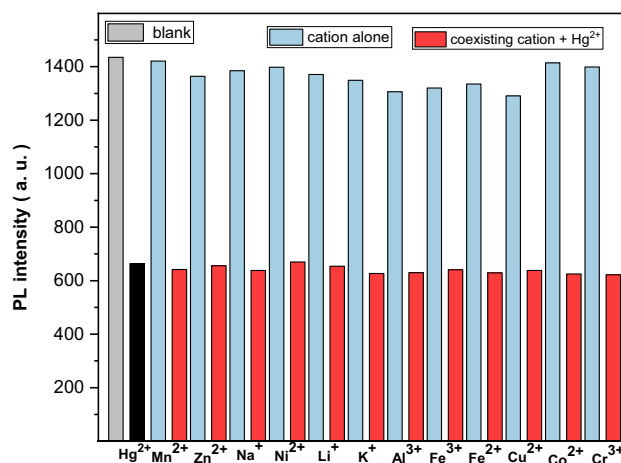


Fig. 13 Various metal ions (10 μM) effect on the PL intensity of CdTe-MSA QDs in the absence and presence of Hg²⁺ ions (3 μM). Excitation at 325 nm, pH = 7.2

Table 4 Different nanoparticle-based fluorescent probes for Hg²⁺ detection

Probe	Linear range	LOD (nM)	Reference
MSA-CdS QDs	[0.1–10 μM]	51	Hosseini and Pirouz (2014)
Carbon dots	[0.1–20 μM]	62	Tabaraki and Sadeghinejad (2018)
CdSe/ZnS QDs	[0.1–100 μM]	90	Li et al. (2021)
CdTe:Ce QDs	[0.01–0.06 μM]	2.6	Chu et al. (2021)
CdTe QDs	[0–0.10 μM]	3.3	Guo et al. (2019)
BSA-Au NCs	[0.2–60 μM]	30	Wang et al. (2016a, b)
Graphene QDs	[0.8–9 μM]	100	Wang et al. (2014)
MSA-CdTe QDs	[0.1–6 μM]	50	This work

Table 5 Analytical performance of the MSA-CdTe probe for Hg²⁺ detection in tap water samples

Samples	Hg ²⁺ added (μM)	Hg ²⁺ found (μM)	Recovery (%)	RSD (%) (n=3)
Tap water	0	Not detected		
	1	0.94	94	4.5
	2	1.95	97.5	2.4
	3	3.11	111.7	3.2
	4	4.07	106.3	2.8

concentrations of Hg²⁺ ions (1, 2, 3 and 4 μM) using the standard addition method. The results are summarized in Table 5.

Hg²⁺ recoveries ranged from 94 to 111.7% with relative standard deviation (RSD) values lower than 5%. These results demonstrate satisfactory reliability and accuracy of the proposed fluorescence probe which can be successfully used for the practical detection of Hg(II) ions in real water samples.

Conclusions

Water soluble CdTe QDs capped with mercaptosuccinic acid (MSA) ligands were prepared by an environmental friendly one-pot hydrothermal synthesis method. Endowed with good spectroscopic properties, this system favors convenient sensing applications based on fluorescence quenching by specific analytes. Under optimal conditions, we have demonstrated an effective CdTe-MSA QDs fluorescence quenching only with Hg²⁺ ions, with little interference effect from other cations. The concentration-dependent fluorescence quenching study by Stern–Volmer model revealed relatively wide linear detection range and low detection limit. The ligation mechanism could be described as a static process by cation binding followed by electron transfer from QDs excited states to mercury ions and competitive cations exchange. Further investigation on this adsorption process by analytical and isotherms

modeling showed that is governed by pseudo-first-order kinetics and conforms to Langmuir and Hill isotherms indicating a monolayer physisorption on homogenous active receptor sites.

The analytical results of probing real water samples are promising for establishing a reliable detection method demonstrating that the prepared CdTe-MSA QDs are potential candidates as highly sensitive and selective fluorescence sensors to detect Hg(II) ions in aqueous solution to counteract environmental pollution.

Acknowledgements This research has been funded by the Deputy for Research & Innovation Ministry of Education through Initiative of Institutional Funding at University of Ha'il—Saudi Arabia through project number IFP-22 083.

Author contributions MA and SB contributed to conceptualization and methodology; MH, FIAA and TYAA contributed to formal analysis, investigation and data curation; MA, FIAA and TYAA contributed to writing—original draft preparation; MA and SB contributed to writing—review and editing; MA involved in supervision; FIAA and TYAA contributed to project administration; FIAA involved in funding acquisition. All authors have read and agreed to the published version of the manuscript.

Funding This research has been funded by the Deputy for Research & Innovation, Ministry of Education through Initiative of Institutional Funding at University of Ha'il—Saudi Arabia through project number IFP-22 083.

Declarations

Conflict of interest The authors declare no competing interests.

Ethical approval Not applicable.

Open Access This article is licensed under a Creative Commons Attribution 4.0 International License, which permits use, sharing, adaptation, distribution and reproduction in any medium or format, as long as you give appropriate credit to the original author(s) and the source, provide a link to the Creative Commons licence, and indicate if changes were made. The images or other third party material in this article are included in the article's Creative Commons licence, unless indicated otherwise in a credit line to the material. If material is not included in the article's Creative Commons licence and your intended use is not permitted by statutory regulation or exceeds the permitted use, you will need to obtain permission directly from the copyright holder. To view a copy of this licence, visit <http://creativecommons.org/licenses/by/4.0/>.

References

- Abdelbar MF, Fayed TA, Meaz TM, Ebeid E-ZM (2016) Photo-induced interaction of thioglycolic acid (TGA)-capped CdTe quantum dots with cyanine dyes. *Spectrochim Acta Part A Mol Biomol Spectrosc* 168:1–11. <https://doi.org/10.1016/j.saa.2016.05.029>
- Abu-Alsoud GF, Hawboldt KA, Bottaro CS (2020) Comparison of four adsorption isotherm models for characterizing molecular recognition of individual phenolic compounds in porous tailor-made molecularly imprinted polymer films. *ACS Appl Mater Interfaces* 12:11998–12009. <https://doi.org/10.1021/acsami.9b21493>
- Algar WR, Krull UJ (2007) Luminescence and stability of aqueous thioalkyl acid capped CdSe/ZnS quantum dots correlated to ligand ionization. *ChemPhysChem* 8:561–568. <https://doi.org/10.1002/cphc.200600686>
- Alibolandi M, Abnous K, Ramezani M, Hosseinkhani H, Hadizadeh F (2014) Synthesis of AS1411-aptamer-conjugated CdTe quantum dots with high fluorescence strength for probe labeling tumor cells. *J Fluoresc* 24:1519–1529. <https://doi.org/10.1007/s10895-014-1437-5>
- Amari A, Elboughdiri N, Ghernaout D, Hadj Lajimi R, Alshahrani AM, Tahoon MA, Ben Rebah F (2021) Multifunctional crosslinked chitosan/nitrogen-doped graphene quantum dot for wastewater treatment. *Ain Shams Eng J* 12(4):4007–4014. <https://doi.org/10.1016/j.asej.2021.02.024>
- Bel Haj Mohamed N, Haouari M, Zaaboub Z, Hassen F, Maaref H, Ben Ouada H (2014) Effect of surface on the optical structure and thermal properties of organically capped CdS nanoparticles. *J Phys Chem Solids* 75:936–944. <https://doi.org/10.1016/j.jpcs.2014.03.007>
- Bel Haj Mohamed N, Ben Brahim N, Mrad R, Haouari M, Ben Chaâbane R, Negrerie M (2018) Use of MPA-capped CdS quantum dots for sensitive detection and quantification of Co^{2+} ions in aqueous solution. *Anal Chim Acta* 1028:50–58. <https://doi.org/10.1016/j.aca.2018.04.041>
- Ben Brahim N, Bel Haj Mohamed N, Poggi M, Ben Chaâbane R, Haouari M, Ben Ouada H, Negrerie M (2017) Interaction of l-cysteine functionalized CdSe quantum dots with metallic cations and selective binding of cobalt in water probed by fluorescence. *Sens Actuators B Chem* 243:489–499. <https://doi.org/10.1016/j.snb.2016.12.003>
- Benjelloun M, Miyah Y, Evrendilek GA, Zerrouq F, Lairini S (2021) Recent advances in adsorption kinetic models: their application to dye types. *Arab J Chem* 14:103031. <https://doi.org/10.1016/j.arabjc.2021.103031>
- Bouazid M, Bouaziz N, Torkia YB, Lamine AB (2019) Statistical physics modeling of ethanol adsorption onto the phenol resin based adsorbents: stereographic, energetic and thermodynamic investigations. *J Mol Liq* 283:674–687. <https://doi.org/10.1016/j.molliq.2019.03.129>
- Brus L (1986) Electronic wave functions in semiconductor clusters: experiment and theory. *J Phys Chem* 90:2555–2560. <https://doi.org/10.1021/j100403a003>
- Cai C, Cheng H, Wang Y, Bao H (2014) Mercaptosuccinic acid modified CdTe quantum dots as a selective fluorescence sensor for Ag^+ determination in aqueous solutions. *RSC Adv* 4:59157–59163. <https://doi.org/10.1039/C4RA07891H>
- Chandan HR, Schiffman JD, Balakrishna RG (2018) Quantum dots as fluorescent probes: synthesis, surface chemistry, energy transfer mechanisms, and applications. *Sens Actuators B Chem* 258:1191–1214. <https://doi.org/10.1016/j.snb.2017.11.189>
- Chen Z, Wu D (2014) Monodisperse BSA-conjugated zinc oxide nanoparticles based fluorescence sensors for Cu^{2+} ions. *Sens Actuators B Chem* 192:83–91. <https://doi.org/10.1016/j.snb.2013.10.092>
- Chu H, Yao D, Chen J, Yu M, Su L (2021) Detection of Hg^{2+} by a dual-fluorescence ratio probe constructed with rare-earth-element-doped cadmium telluride quantum dots and fluorescent carbon dots. *ACS Omega* 6:10735–10744. <https://doi.org/10.1021/acscomega.1c00263>
- Das D, Dutta RK (2021) Photoluminescence lifetime based nickel ion detection by glutathione capped CdTe/CdS core-shell quantum dots. *J Photochem Photobiol A* 416:113323. <https://doi.org/10.1016/j.jphotochem.2021.113323>
- Delehanty JB, Bradburne CE, Susumu K, Boeneman K, Mei BC, Farrell D, Blanco-Canosa JB, Dawson PE, Mattoussi H, Medintz IL (2011) Spatiotemporal multicolor labeling of individual cells using peptide-functionalized quantum dots and mixed delivery techniques. *J Am Chem Soc* 133:10482–10489. <https://doi.org/10.1021/ja200555z>
- Deng S, Long J, Dai X, Wang G, Zhou L (2023) Simultaneous detection and adsorptive removal of Cr(VI) ions by fluorescent sulfur quantum dots embedded in chitosan hydrogels. *ACS Appl Nano Mater* 6:1817–1827. <https://doi.org/10.1021/acsnm.2c04768>
- Ding R, Cheong YH, Ahamed A, Lisak G (2021) Heavy metals detection with paper-based electrochemical sensors. *Anal Chem* 93:1880–1888. <https://doi.org/10.1021/acs.analchem.0c04247>
- Du W, Liao L, Yang L, Qin A, Liang A (2017) Aqueous synthesis of functionalized copper sulfide quantum dots as near-infrared luminescent probes for detection of Hg^{2+} , Ag^+ and Au^{3+} . *Sci Rep* 7:11451. <https://doi.org/10.1038/s41598-017-10904-y>
- Dutta P, Saikia D, Adhikary NC, Sarma NS (2015) Macromolecular systems with MSA-capped CdTe and CdTe/ZnS core/shell quantum dots as superselective and ultrasensitive optical sensors for picric acid explosive. *ACS Appl Mater Interfaces* 7:24778–24790. <https://doi.org/10.1021/acscami.5b07660>
- El-Nahass MM, Youssef GM, Noby SZ (2014) Structural and optical characterization of CdTe quantum dots thin films. *J Alloy Compd* 604:253–259. <https://doi.org/10.1016/j.jallcom.2014.03.104>
- Ensafi AA, Kazemifard N, Rezaei B (2016) A simple and sensitive fluorimetric aptasensor for the ultrasensitive detection of arsenic(III) based on cysteamine stabilized CdTe/ZnS quantum dots aggregation. *Biosens Bioelectron* 77:499–504. <https://doi.org/10.1016/j.bios.2015.10.011>
- Foo KY, Hameed BH (2010) Insights into the modeling of adsorption isotherm systems. *Chem Eng J* 156:2–10. <https://doi.org/10.1016/j.cej.2009.09.013>
- Freundlich H (1907) Über die adsorption in Lösungen. *Z FürPhysChem* 57:385–470. <https://doi.org/10.1515/zpch-1907-5723>
- Gan T-T, Zhang Y-J, Zhao N-J, Xiao X, Yin G-F, Yu S-H, Wang H-B, Duan J-B, Shi C-Y, Liu W-Q (2012) Hydrothermal synthetic mercaptopropionic acid stabled CdTe quantum dots as fluorescent probes for detection of Ag^+ . *Spectrochim Acta Part A Mol Biomol Spectrosc* 99:62–68. <https://doi.org/10.1016/j.saa.2012.09.005>
- García De Arquer FP, Talapin DV, Klimov VI, Arakawa Y, Bayer M, Sargent EH (2021) Semiconductor quantum dots: technological progress and future challenges. *Science* 373:eaz8541. <https://doi.org/10.1126/science.aaz8541>
- Gogoi M, Deb P, Kostka A (2012) Differential tunability effect on the optical properties of doped and undoped quantum dots: optical properties of doped and undoped quantum dots. *Phys Status Solidi A* 209:1543–1551. <https://doi.org/10.1002/pssa.201228074>
- Gong T, Liu J, Liu X, Liu J, Xiang J, Wu Y (2016) A sensitive and selective sensing platform based on CdTe QDs in the presence of l-cysteine for detection of silver, mercury and copper ions in water and various drinks. *Food Chem* 213:306–312. <https://doi.org/10.1016/j.foodchem.2016.06.091>
- Guo H, Li J, Li Y, Wu D, Ma H, Wei Q, Du B (2019) Exciton energy transfer-based fluorescent sensor for the detection of Hg^{2+} through aptamer-programmed self-assembly of QDs. *Anal Chim Acta* 1048:161–167. <https://doi.org/10.1016/j.aca.2018.10.021>

- Hao L, Shen Y, Chen X, Yang X, Du Q, Bian Y, Chen L, Tang K, Zhang R, Zheng Y, Gu S (2019) Different-sized CdTe QDs on the detection of Cu^{2+} ions: combining experimental investigation with first-principles verification. *Microchem J* 148:684–690. <https://doi.org/10.1016/j.microc.2019.05.048>
- He Y, Wang Y, Mao G, Liang C, Fan M (2022) Ratiometric fluorescent nanoprobe based on carbon dots and multicolor CdTe quantum dots for multiplexed determination of heavy metal ions. *Anal Chim Acta* 1191:339251. <https://doi.org/10.1016/j.aca.2021.339251>
- Hoang Q-B, Nguyen T-N, Nguyen T-P, Nguyen A-D, Chu N-H, Ta V-T, Nguyen V-H, Mai X-D (2022) Size-dependent reactivity of highly photoluminescent CdZnTeS alloyed quantum dots to mercury and lead ions. *Chem Phys* 552:111378. <https://doi.org/10.1016/j.chemphys.2021.111378>
- Hosseini MS, Pirouz A (2014) Study of fluorescence quenching of mercaptosuccinic acid-capped CdS quantum dots in the presence of some heavy metal ions and its application to Hg(II) ion determination: fluorescence quenching of MSA-capped CdS QDs. *Luminescence* 29:798–804. <https://doi.org/10.1002/bio.2623>
- Järup L (2003) Hazards of heavy metal contamination. *Br Med Bull* 68:167–182. <https://doi.org/10.1093/bmb/ldg032>
- Kalasad MN, Rabinal MK, Mulimani BG (2010) Facile synthesis of bioconjugated fluorescent CdS nanoparticles of tunable light emission. *J Phys D Appl Phys* 43:305301. <https://doi.org/10.1088/0022-3727/43/30/305301>
- Kapitonov AM, Stupak AP, Gaponenko SV, Petrov EP, Rogach AL, Eychmüller A (1999) Luminescence properties of thiol-stabilized CdTe nanocrystals. *J Phys Chem B* 103:10109–10113. <https://doi.org/10.1021/jp9921809>
- Ke J, Li X, Zhao Q, Hou Y, Chen J (2014) Ultrasensitive quantum dot fluorescence quenching assay for selective detection of mercury ions in drinking water. *Sci Rep* 4:5624. <https://doi.org/10.1038/srep05624>
- Labe M, Sakr A-H, Soliman M, Abdel-Fattah TM, Ebrahim S (2018) Effect of capping agent on selectivity and sensitivity of CdTe quantum dots optical sensor for detection of mercury ions. *Opt Mater* 79:331–335. <https://doi.org/10.1016/j.optmat.2018.03.060>
- Langmuir I (2018) The adsorption of gases on plane surfaces of glass, mica and platinum. *J Am Chem Soc* 40:1361–1403. <https://doi.org/10.1021/ja02242a004>
- Leitzke TJ, Downey J, LaDouceur RM, Margrave DM, Wallace GC, Hutchins DL (2022) Water treatment method for removal of select heavy metals and nutrient ions through adsorption by magnetite. *ACS EST Water* 2:1584–1592. <https://doi.org/10.1021/acsestwater.2c00242>
- Li H, Wang W, Wang Z, Lu Q, Bai H, Zhang Q (2021) Analyte-enhanced photocatalytic activity of CdSe/ZnS quantum dots for paper-based colorimetric sensing of Hg^{2+} under visible light. *Microchem J* 164:106037. <https://doi.org/10.1016/j.microc.2021.106037>
- Liu I-S, Lo H-H, Chien C-T, Lin Y-Y, Chen C-W, Chen Y-F, Su W-F, Liou S-C (2008) Enhancing photoluminescence quenching and photoelectric properties of CdSe quantum dots with hole accepting ligands. *J Mater Chem* 18:675. <https://doi.org/10.1039/b715253a>
- Lou Y, Zhao Y, Chen J, Zhu J-J (2014) Metal ions optical sensing by semiconductor quantum dots. *J Mater Chem c* 2:595–613. <https://doi.org/10.1039/C3TC31937G>
- Mahmoud ME, Fekry NA, Abdelfattah AM (2022) Engineering nanocomposite of graphene quantum dots/carbon foam/alginate/zinc oxide beads for efficacious removal of lead and methylene. *J Ind Eng Chem* 115:365. <https://doi.org/10.1016/j.jiec.2022.08.020>
- Ouni S, Bel Haj Mohamed N, Chaaben N, Bonilla-Petriciolet A, Haouari M (2022) Fast and effective catalytic degradation of an organic dye by eco-friendly capped ZnS and Mn-doped ZnS nanocrystals. *Environ Sci Pollut Res* 29:33474–33494. <https://doi.org/10.1007/s11356-021-17860-1>
- Pang X, Bouzid M, Dos Santos JMN (2020) Theoretical study of indigotine blue dye adsorption on CoFe_2O_4 /chitosan magnetic composite via analytical model. *Colloids Surf Physicochem Eng Asp* 589:124467. <https://doi.org/10.1016/j.colsurfa.2020.124467>
- Pei J, Zhu H, Wang X, Zhang H, Yang X (2012) Synthesis of cysteamine-coated CdTe quantum dots and its application in mercury (II) detection. *Anal Chim Acta* 757:63–68. <https://doi.org/10.1016/j.aca.2012.10.037>
- Pejjai B, Minnam Reddy VR, Seku K, Kotte TRR, Park C (2017) Chemical bath deposition of Mn-doped ZnS thin films using greener complexing agents: effect of Mn-doping on the optical properties. *Optik* 130:608–618. <https://doi.org/10.1016/j.ijleo.2016.10.083>
- Peng C-F, Zhang Y-Y, Qian Z-J, Xie Z-J (2018) Fluorescence sensor based on glutathione capped CdTe QDs for detection of Cr^{3+} ions in vitamins. *Food Sci Hum Wellness* 7:71–76. <https://doi.org/10.1016/j.fshw.2017.12.001>
- Preeyanka N, Sarkar M (2021) Probing How various metal ions interact with the surface of QDs: implication of the interaction event on the photophysics of QDs. *Langmuir* 37:6995–7007. <https://doi.org/10.1021/acs.langmuir.1c00548>
- Ragadhita R, Nandiyanto ABD (2021) How to calculate adsorption isotherms of particles using two-parameter monolayer adsorption models and equations. *Indones J Sci Technol* 6(1):205–234
- Redlich O, Peterson DL (1959) A useful adsorption isotherm. *J Phys Chem* 63:1024–1024. <https://doi.org/10.1021/j150576a611>
- Ribeiro DSM, Castro RC, Páscoa RNMJ, Soares JX, Rodrigues SSM, Santos JLM (2019) Tuning CdTe quantum dots reactivity for multipoint detection of mercury(II), silver(I) and copper(II). *J Lumin* 207:386–396. <https://doi.org/10.1016/j.jlumin.2018.11.035>
- Saikia D, Dutta P, Sarma NS, Adhikary NC (2016) CdTe/ZnS core/shell quantum dot-based ultrasensitive PET sensor for selective detection of Hg (II) in aqueous media. *Sens Actuators B Chem* 230:149–156. <https://doi.org/10.1016/j.snb.2016.02.035>
- Shenouda AY, El Sayed EM (2015) Electrodeposition, characterization and photo electrochemical properties of CdSe and CdTe. *Ain Shams Eng J* 6:341–346. <https://doi.org/10.1016/j.asej.2014.07.010>
- Shrivastava A, Gupta V (2011) Methods for the determination of limit of detection and limit of quantitation of the analytical methods. *Chron Young Sci* 2:21. <https://doi.org/10.4103/2229-5186.79345>
- Shu J, Tang D (2020) Recent advances in photoelectrochemical sensing: from engineered photoactive materials to sensing devices and detection modes. *Anal Chem* 92:363–377. <https://doi.org/10.1021/acs.analchem.9b04199>
- Singh S, Vaishnav JK, Mukherjee TK (2020) Quantum dot-based hybrid coacervate nanodroplets for ultrasensitive detection of Hg^{2+} . *ACS Appl Nano Mater* 3:3604–3612. <https://doi.org/10.1021/acsnano.0c00317>
- Sitko R, Janik P, Zawisza B, Talik E, Margui E, Queralt I (2015) Green approach for ultratrace determination of divalent metal ions and arsenic species using total-reflection X-ray fluorescence spectrometry and mercapto-modified graphene oxide nanosheets as a novel adsorbent. *Anal Chem* 87:3535–3542. <https://doi.org/10.1021/acs.analchem.5b00283>
- Smith AM, Mohs AM, Nie S (2009) Tuning the optical and electronic properties of colloidal nanocrystals by lattice strain. *Nat Nanotechnol* 4:56–63. <https://doi.org/10.1038/nnano.2008.360>
- Sousa JCL, Vivas MG, Vale BRC, Ferrari JL, Schiavon DMA (2018) Effect of mercaptosuccinic acid stabilizer agent on the optical properties of colloidal CdTe quantum dots. *J Nanosci Nanotechnol* 18:651–658. <https://doi.org/10.1166/jnn.2018.13932>
- Tabaraki R, Sadeghinejad N (2018) Microwave assisted synthesis of doped carbon dots and their application as green and simple turn

- off-on fluorescent sensor for mercury (II) and iodide in environmental samples. *Ecotoxicol Environ Saf* 153:101–106. <https://doi.org/10.1016/j.ecoenv.2018.01.059>
- Tauc J, Mentha A (1972) States in the gap. *J Non-Cryst Solids* 8–10:569–585. [https://doi.org/10.1016/0022-3093\(72\)90194-9](https://doi.org/10.1016/0022-3093(72)90194-9)
- Vinoth Kumar GG, Kesavan MP, Tamilselvi A, Rajagopal G, Raja JD, Sakthipandi K, Rajesh J, Sivaraman G (2018) A reversible fluorescent chemosensor for the rapid detection of Hg²⁺ in an aqueous solution: its logic gates behavior. *Sens Actuators B Chem* 273:305–315. <https://doi.org/10.1016/j.snb.2018.06.067>
- Wang Y-Q, Ye C, Zhu Z-H, Hu Y-Z (2008) Cadmium telluride quantum dots as pH-sensitive probes for tiopronin determination. *Anal Chim Acta* 610:50–56. <https://doi.org/10.1016/j.aca.2008.01.015>
- Wang B, Zhuo S, Chen L, Zhang Y (2014) Fluorescent graphene quantum dot nanoprobe for the sensitive and selective detection of mercury ions. *Spectrochim Acta Part A Mol Biomol Spectrosc* 131:384–387. <https://doi.org/10.1016/j.saa.2014.04.129>
- Wang H, Zhu W, Fang M, Xu Y, Li C (2016a) Turn-on fluorescence probe for high sensitive and selective detection of Ag⁺ by L-glutathione capped CdTe quantum dots in aqueous medium. *J Lumin* 180:14–19. <https://doi.org/10.1016/j.jlumin.2016.07.049>
- Wang Y-W, Tang S, Yang H-H, Song H (2016b) A novel colorimetric assay for rapid detection of cysteine and Hg²⁺ based on gold clusters. *Talanta* 146:71–74. <https://doi.org/10.1016/j.talanta.2015.08.015>
- Wei X, Zhou Z, Hao T, Li H, Dai J, Gao L, Zheng X, Wang J, Yan Y (2015) Simple synthesis of thioglycolic acid-coated CdTe quantum dots as probes for Norfloxacin lactate detection. *J Lumin* 161:47–53. <https://doi.org/10.1016/j.jlumin.2014.12.050>
- Wu D, Chen Z, Huang G, Liu X (2014a) ZnSe quantum dots based fluorescence sensors for Cu²⁺ ions. *Sens Actuators A* 205:72–78. <https://doi.org/10.1016/j.sna.2013.10.020>
- Wu P, Zhao T, Wang S, Hou X (2014b) Semiconductor quantum dots-based metal ion probes. *Nanoscale* 6:43–64. <https://doi.org/10.1039/C3NR04628A>
- Xia Y, Zhu C (2007) Use of surface-modified CdTe quantum dots as fluorescent probes in sensing mercury (II). *Talanta*. <https://doi.org/10.1016/j.talanta.2007.11.008>
- Xu M, Wang X, Liu X (2022) Detection of heavy metal ions by ratio-metric photoelectric sensor. *J Agric Food Chem* 70:11468–11480. <https://doi.org/10.1021/acs.jafc.2c03916>
- Yusuff AS, Popoola LT, Babatunde EO (2019) Adsorption of cadmium ion from aqueous solutions by copper-based metal organic framework: equilibrium modeling and kinetic studies. *Appl Water Sci* 9:106. <https://doi.org/10.1007/s13201-019-0991-z>
- Zhou H, Yang C, Liao M, Li M, Diao N, Wu S, Wang J (2022) Exploring the mechanism of CdTe quantum dots as fluorescent probe to detect Hg(II) ion from the perspectives of fluorescence polarization and light scattering. *Chem Phys Lett* 792:139415. <https://doi.org/10.1016/j.cplett.2022.139415>

Publisher's Note Springer Nature remains neutral with regard to jurisdictional claims in published maps and institutional affiliations.